Published in final edited form as:
Neuroimage. 2010 August 1; 52(1): 290–301. doi:10.1016/j.neuroimage.2010.04.009.

Development of functional and structural connectivity within the default mode network in young children

Kaustubh Supekar[1,2], **Lucina Q. Uddin**[3], **Katherine Prater**[3], **Hitha Amin**[3], **Michael D. Greicius**[4], and **Vinod Menon**[3,4,5]

[1]Graduate Program in Biomedical Informatics, Stanford University School of Medicine, Stanford, CA 94304

[2]Center for Biomedical Informatics Research, Stanford University School of Medicine, Stanford, CA 94304

[3]Department of Psychiatry & Behavioral Sciences, Stanford University School of Medicine, Stanford, CA 94304

[4]Neurology and Neurological Sciences, Stanford University School of Medicine, Stanford, CA 94304

[5]Program in Neuroscience, Stanford University School of Medicine, Stanford, CA 94304

Abstract

Functional and structural maturation of networks comprised of discrete regions is an important aspect of brain development. The default-mode network (DMN) is a prominent network which includes the posterior cingulate cortex (PCC), medial prefrontal cortex (mPFC), medial temporal lobes (MTL), and angular gyrus (AG). Despite increasing interest in DMN function, little is known about its maturation from childhood to adulthood. Here we examine developmental changes in DMN connectivity using a multimodal imaging approach by combining resting-state fMRI, voxel-based morphometry and diffusion tensor imaging-based tractography. We found that the DMN undergoes significant developmental changes in functional and structural connectivity, but these changes are not uniform across all DMN nodes. Convergent structural and functional connectivity analyses suggest that PCC-mPFC connectivity along the cingulum bundle is the most immature link in the DMN of children. Both PCC and mPFC also showed gray matter volume differences, as well as prominent macrostructural and microstructural differences in the dorsal cingulum bundle linking these regions. Notably, structural connectivity between PCC and left MTL was either weak or non-existent in children, even though functional connectivity did not differ from that of adults. These results imply that functional connectivity in children can reach adult-like levels despite weak structural connectivity. We propose that maturation of PCC-mPFC structural connectivity plays an important role in the development of self-related and social-cognitive functions that emerge during adolescence. More generally, our study demonstrates how quantitative multimodal analysis of anatomy and connectivity allows us to better characterize the heterogeneous development and maturation of brain networks.

Corresponding Authors Kaustubh Supekar and Vinod Menon, 780 Welch Road, Room 201, Stanford University School of Medicine, Stanford, CA 94304, tel: 1-650-736-0128, fax: 1-650-736-7200, (ksupekar@stanford.edu or menon@stanford.edu).

Keywords

brain development; default mode network; DTI; functional brain connectivity; structural brain connectivity

Introduction

There is growing scientific interest in understanding large-scale brain networks that underlie higher-level cognition in humans. The default-mode network (DMN) is a prominent large-scale brain network that includes the posterior cingulate cortex (PCC), medial prefrontal cortex (mPFC), medial temporal lobes (MTL), and angular gyrus (AG). The DMN is unique in terms of its high resting metabolism, deactivation profile during cognitively demanding tasks (Raichle et al., 2001; Shulman et al., 1997), and increased activity during high-level social cognitive tasks (Harrison et al., 2008). The precise functions collectively subserved by the DMN are still largely unknown, but the individual brain regions comprising it are involved in integration of autobiographical, self-monitoring and social cognitive functions (Spreng et al., 2009). The PCC is activated during tasks that involve autobiographical memory and self-referential processes (Buckner and Carroll, 2007), the mPFC is associated with social cognitive processes related to self and others (Amodio and Frith, 2006), the MTL is engaged in episodic memory (Milner, 2005), and the AG is implicated in semantic processing and attention (Binder et al., 2009; Chambers et al., 2004). Regardless of the specific functions subserved by each region of the DMN, it is noteworthy that dynamic suppression of this network during cognitively demanding tasks appears to be necessary for accurate behavioral performance (Kelly et al., 2008; Polli et al., 2005; Weissman et al., 2006).

Most of our knowledge about the DMN has been based on brain imaging studies in adults. In adults, the DMN can be reliably isolated in virtually every individual, presumably because interactions between the core brain regions that comprise it have led to a stable and mature network. Very little is currently known about the functional maturation of the DMN from childhood to adulthood, and less is known about structural changes that underlie the functional maturation of the DMN. Notably, no study has examined white matter within the DMN in children, using diffusion tensor imaging (DTI) tractography. As a result, the relationship between DMN structure and function in children is also not known. Examining the developmental trajectory of the DMN is important not only for understanding how structural brain changes during development impact development of key functional brain circuits, but also for understanding the ontogeny of cognitive processes subserved by the DMN. Additionally, the putative functions of the DMN, as well as the maturation of cognitive control mechanisms, are relatively late to develop in children, and are often compromised in neurodevelopmental disorders such as autism spectrum disorders and attention-deficit/hyperactivity disorder (Broyd et al., 2009).

Here we use resting-state fMRI in conjunction with DTI and optimized voxel-based morphometry (VBM) to characterize functional, white matter, and gray matter changes within the DMN from childhood to young adulthood. Specifically, we investigated developmental changes in functional and structural connectivity between key nodes within the DMN. We additionally examined the relationship between measures of functional and structural connectivity between DMN regions. Previous structural neuroimaging studies have shown that while gray matter volume follows a regionally specific inverted U-shaped trajectory, white matter volume shows protracted increases with development (Lenroot and Giedd, 2006). This principle suggests that connectivity between different cortical regions matures at different time points during development (Gogtay, 2004). We therefore hypothesized that DMN maturation would be characterized by heterogeneous changes in structural and functional connectivity

with age. We further hypothesized that weak long-range structural connections between the PCC and the mPFC would have a significant impact on functional connectivity in children.

Materials and Methods

Participants

Twenty-three children and twenty-two IQ-matched young-adult subjects participated in this study after providing written informed consent. For those subjects who were unable to give informed consent, written informed consent was obtained from their legal guardian. The study protocol was approved by the Stanford University Institutional Review Board. The child subjects (10 males, 13 females) ranged in age from 7 to 9 (mean age 7.95) with an IQ range of 88 to 137 (mean IQ: 112). The young-adult subjects (11 males, 11 females) ranged in age from 19 to 22 (mean age 20.4) with an IQ range of 97 to 137 (mean IQ: 112). The subjects were recruited locally – children from local schools and young-adult subjects from Stanford University and neighboring community colleges. Eleven of the 23 child subjects were 2nd graders; twelve of the child subjects were 3rd graders. The young-adult subjects had received 13 to 16 years of education (mean years of education 14.5), Table 1.

Functional MRI

Data acquisition—For the task-free scan, subjects were instructed to keep their eyes closed and try not to move for the duration of the 8 minute scan. Functional Images were acquired on a 3T GE Signa scanner (General Electric, Milwaukee, WI) using a custom-built head coil. Head movement was minimized during scanning by a comfortable custom-built restraint. A total of 29 axial slices (4.0mm thickness, 0.5mm skip) parallel to the AC-PC line and covering the whole brain were imaged with a temporal resolution of 2 seconds using a T2* weighted gradient echo spiral in-out pulse sequence (Glover and Law, 2001) with the following parameters: TR = 2000msec, TE = 30msec, flip angle = 80°, 1 interleave. The field of view was 20 cm, and the matrix size was 64×64, providing an in-plane spatial resolution of 3.125 mm. To reduce blurring and signal loss arising from field inhomogeneities, an automated high-order shimming method based on spiral acquisitions was used before acquiring functional MRI scans.

Data preprocessing—The first 5 volumes were not analyzed to allow for signal equilibration effects. A linear shim correction was applied separately for each slice during reconstruction using a magnetic field map acquired automatically by the pulse sequence at the beginning of the scan (Glover and Lai, 1998). Functional MRI data were then analyzed using SPM5 analysis software (http://www.fil.ion.ucl.ac.uk/spm). Images were realigned to correct for motion, corrected for errors in slice-timing, spatially transformed to standard stereotaxic space (based on the Montreal Neurologic Institute (MNI) coordinate system), resampled every 2 mm using sinc interpolation and smoothed with a 6mm full-width half-maximum Gaussian kernel to decrease spatial noise prior to statistical analysis. Translational movement in millimeters (x, y, z) and rotational motion in degrees (pitch, roll, yaw) was calculated based on the SPM5 parameters for motion correction of the functional images in each subject. No participants had a range of movement greater than 3mm translation or 3 degrees of rotation. A two-sample t-test revealed that motion parameters did not differ between children and young adults ($p < 0.01$), Table 2.

Group ICA analysis—Each participant's smoothed, normalized images were concatenated across time to form a four dimensional matrix using FSL 3.3. This four dimensional matrix was then analyzed with FSL 4.4 melodic ICA concatenated across participants. This analysis was limited to output only 25 components for the group. From these components, the default mode network (DMN) was selected for subsequent analyses using previously validated methods (Greicius et al., 2004). In addition to the DMN, five other networks (salience network,

right executive control network, left executive control network (ECN), visual, and sensorimotor network) – were also selected based on their consistent identification across a number of research studies (Biswal et al., 1995; Damoiseaux et al., 2006; De Luca et al., 2005; Greicius et al., 2003; Seeley et al., 2007). . All components were then binarized using SPM5 in order to create templates for choosing network components for each individual (Greicius et al. 2003), as described below.

Individual subject analyses—Each participant's smoothed, normalized, four dimensional matrix was analyzed with FSL melodic ICA version 12. The number of components output by ICA was determined automatically by the PCA process of the melodic software. For young adults, the number of ICA components generated ranged from 23 to 93. For children, the number of ICA components generated ranged from 45 to 74. Children and young adults did not differ in the number of ICA components generated. The templates created above for the six networks were then applied to each participant's individual ICA components to select the "best-fit" network component. To do this, we developed a nonlinear template-matching procedure that involved taking the average z-score of voxels falling within the template minus the average z-score of voxels outside the template and selecting the component in which this difference (the goodness-of-fit) was the greatest. Z-scores here reflect the degree to which a given voxel's time series correlates with the time series corresponding to the specific ICA component. This method allowed us to select each individual's DMN, salience, right ECN, left ECN, visual and sensorimotor network.

Group analyses—Within-group, between-group, and combined-group analyses were performed using the individual best-fit network components for the DMN network. Individual *t*-statistics images were used to determine group-level statistical maps using a one sample t-test as implemented in SPM5. Between-group differences were determined using a two sample t-test. The within-group analysis was masked with a skull-stripped binary image of the standard MNI T1; the between-group analysis was masked with a positive only mask of the two groups combined. Significant clusters were determined using a voxel-wise statistical height ($p < 0.01$) and extent ($p < 0.01$) thresholds, corrected at the whole-brain level.

Regions of Interest Selection—ROIs were selected from combined-group clusters in the PCC, mPFC, bilateral MTL, and bilateral angular gyrus. The PCC and mPFC ROIs spanned both hemispheres. After visually selecting a voxel with the highest *Z* score within each cluster on the functional map, the final ROIs were constructed by drawing spheres with centers as the seed-point and a radius of 8mm. This ROI selection procedure is widely used in extant resting-state functional connectivity studies (Fair et al., 2008; Fox et al., 2005; Kelly et al., 2009).

Functional Connectivity—The regional resting-state fMRI timeseries was computed for each of the ROIs by averaging all the voxels within each region at each timepoint in the timeseries, resulting in 235 time points for each of the four DMN regions. Using a similar method, representative resting-state network (RSN) fMRI timeseries for the salience, right ECN, left ECN, visual and sensorimotor networks were computed. These regional and RSN timeseries were temporally filtered using a bandpass filter ($0.0083 \text{ Hz} < f < 0.15 \text{ Hz}$). We used partial correlation as a measure of strength of functional connectivity between brain regions belonging to the DMN. Specifically, we computed functional connectivity as partial correlations controlling for the influence of other DMN nodes and five other major large-scale brain networks. Partial correlation measures the degree of association between two regions, controlling for the effect of other regions, and has been widely used in task- and resting-state fMRI (Liu et al., 2008; Salvador et al., 2005; Sun et al., 2004; van den Heuvel et al., 2008). As noted by van den Heuvel and colleagues (van den Heuvel et al., 2008), this partial correlation approach has significant advantages over the pure correlation approach employed in previous

studies. In particular, our analysis allows the investigation of functional connectivity uncontaminated by activity in the nodes of the five other major networks. To account for the non-normality of partial correlations, a Fisher's r-to-z transform was applied.

Structural MRI

Data acquisition—For each subject, a high resolution T1-weighted spoiled grass gradient recalled (SPGR) inversion recovery 3D MRI sequence was acquired to facilitate anatomical localization of functional data and for performing anatomical morphometric analyses. The following parameters were used: TI = 300 msec, TR = 8.4 msec; TE = 1.8 msec; flip angle = 15°; 22 cm field of view; 132 slices in coronal plane; 256 × 192 matrix; 2 NEX, acquired resolution = 1.5 × 0.9 × 1.1 mm. Structural and functional images were acquired in the same scan session.

Voxel-based morphometry—Voxel-wise differences in brain anatomy within DMN regions were assessed using the optimized voxel-based morphometry (VBM) method (Good et al., 2001). This analysis was performed with the VBM5 toolbox developed by Christian Gaser (University of Jena, Germany, http://dbm.neuro.uni-jena.de/vbm). Prior to analyses, the structural images were resliced with trilinear interpolation to isotropic 1×1×1 voxels and aligned to conventional AC-PC space, using manually identified landmarks, including the anterior commissure (AC), the posterior commissure (PC) and the mid-sagittal plane. The resliced images were spatially normalized to the Montreal Neurological Institute (MNI) stereotactic space. Spatial transformation was nonlinear with warping regularization=1; warp frequency cutoff=25. The spatially normalized images were then segmented into gray matter (GM), white matter (WM), and cerebrospinal fluid (CSF) compartments, with a modified mixture model cluster analysis technique (Good et al., 2001) with the following parameters: bias regularization=0.0001, bias FWHM cutoff=70mm, sampling distance=3, HMRF weighting=0.3. As recommended by Gaser et al. for children or elderly populations, we used no tissue priors for segmentation. Voxel values were modulated by the Jacobian determinants derived from the spatial normalization such that areas that were expanded during warping were proportionally reduced in intensity. We used modulation for nonlinear effects only (while the warping included both an affine and a nonlinear component). When using modulated images for performing subsequent group comparisons, the inference is made on measures of volume rather than tissue concentration (density). The use of modulation for nonlinear but not affine effects ensures that the statistical comparisons are made on relative (e.g. while controlling for overall brain size) rather than absolute volumes.

The segmented (modulated) images for white and gray matter were smoothed with an isotropic Gaussian kernel (10 mm full width at half maximum). The size of the kernel for smoothing was chosen as recommended by Gaser et al. for modulated images, since modulation introduces additional smoothing. Between-group comparisons for gray and white matter separately were performed in SPM5 as two-sample t-tests on smoothed images. The results presented here were visualized at height threshold of $p < 0.001$ (uncorrected), and non-stationary cluster extent threshold (Hayasaka et al., 2004) of $p < 0.001$ with family-wise error correction for multiple comparisons. The gray matter results pertaining to the DMN were determined by masking the gray matter results volume with the combined-group DMN ICA maps. Similarly, white matter results pertaining to the DMN were determined by masking the white matter results volume with the cingulum fibers volume extracted from the adult DTI atlas published by the International Consortium of Brain Mapping (ICBM) (ICBM-DTI-81 atlas, http://www.loni.ucla.edu/Atlases).

Diffusion Tensor Imaging

Data acquisition—DTI data was obtained from 18 of the 23 children subjects and 15 of 22 young adults. The DTI pulse sequence was a diffusion-weighted single-shot spin-echo, echo planar imaging sequence (TE = 70.8 ms; TR = 8.6 s; field of view = 220 mm; matrix size = 128 × 128; bandwidth = ±110kHz; partial k-space acquisition). We acquired 63 axial, 2-mm thick slices (no skip) for 2 *b* values, b = 0 and b = approximately 850 s/mm^2. The high b value was obtained by applying gradients along 23 different diffusion directions. Two gradient axes were energized simultaneously to minimize TE. The polarity of the effective diffusion-weighting gradients was reversed for odd repetitions to reduce cross-terms between diffusion gradients and imaging and background gradients. Although Jones (Jones, 2004) suggests that measuring more diffusion directions would be a more efficient way to reliably estimate diffusion tensors of arbitrary orientation, our signal-to-noise ratio is sufficiently high from our 4 repeats to produce very reliable tensor estimates suitable for tractography.

Data preprocessing—DTI data were preprocessed using a custom program based on normalized mutual information that removed eddy current distortion effects and determined a constrained nonrigid image registration of all the diffusion images (Bammer et al., 2002). The 6 elements of the diffusion tensor were determined by multivariate regression (Basser, 1995; Basser and Pierpaoli, 1996). For each subject, the non–diffusion-weighted ($b = 0$) images were coregistered to the T1-weighted 3-D SPGR anatomical images using a mutual information 3-D rigid-body coregistration algorithm from SPM5. Several anatomical landmarks, including the anterior commissure (AC), the posterior commissure (PC), and the midsagittal plane, were identified by hand in the T1 images. With these landmarks, we computed a rigid-body transform from the native image space to the conventional AC-PC–aligned space. The DTI data were then resampled to this AC-PC–aligned space with 2-mm isotropic voxels using a spline-based tensor interpolation algorithm (Pajevic et al., 2002), taking care to rotate the tensors to preserve their orientation with respect to the anatomy (Alexander et al., 2001). The T1 images were resampled to AC-PC–aligned space with 1-mm isotropic voxels. We confirmed by visual inspection of each dataset that this coregistration technique aligns the DTI and T1 images to within 1–2 millimeters in the brain regions of interest.

Tractography—Using custom DTI analysis software (available for download at http://sirl.stanford.edu/software/), the tractography procedure was initiated by whole-brain fiber tracking in native space that produced many fiber paths. The spatially normalized PCC, mPFC, and bilateral MTL ROIs obtained from the combined-group ICA DMN maps were then warped back to each individual brain to be used for the subsequent DTI tractography analyses. This was done by applying the inverse of the spatial normalization transformation. As fiber tracking becomes unreliable in gray matter, we ensured that our ROIs extended 2–3mm into the white matter. Tracts that did not end in or pass through both ROIs were discarded. For the larger PCC and mPFC ROIs, tracts were only kept if they ended in the ROI. Each fiber tract was estimated using a deterministic streamlines tracking algorithm (Basser et al., 2000; Conturo et al., 1999; Mori et al., 1999) with a fourth order Runge-Kutta path integration method (Press, 2002) and 1 mm fixed step size. A continuous tensor field was estimated using trilinear interpolation of the tensor elements. Starting from the initial seed point, fiber paths were traced in both directions along the principal diffusion axis. Path tracing proceeded until the FA fell below 0.15 or until the minimum angle between the current and previous path segments was larger than 30°. To limit the number of false positives, fibers that were anatomically implausible were identified visually and removed.

Structural connectivity—For each subject, the density of the fibers connecting the PCC to the mPFC, PCC to MTL, and mPFC to MTL was measured, in native space. The density of fibers (number of fibers per unit area) connecting two regions *u* and *v* was computed as

$$\text{fiber-density}(u,v)=\frac{2}{Su+Sv}\sum_{f\in F(u,v)}\frac{1}{l(f)} \quad (1)$$

where F(u,v) is a set of all the fibers connecting u and v, l(f) length of the individual fiber, Su and Sv are sizes of the ROIs (Hagmann et al., 2008). The fiber density, a measure of structural connectivity, describes the fiber tracts interconnecting the regions of interest. Additionally, fiber mean fractional anisotropy (FA) was computed by averaging FA values along the tract. FA is a measure of organization of the underlying white matter(Beaulieu, 2002). Both fiber density and mean FA have been used previously to quantify structural connectivity, particularly to characterize white matter integrity (Hagmann et al., 2008; van den Heuvel et al., 2008). In our study, we used fiber density and mean FA as a measure of the integrity of the fiber tracts connecting DMN brain regions.

The structural connectivity analyses described above were repeated on an independent dataset of 10 healthy children (see Results section for details).

Results

Demographic data is shown in Table 1. Participant groups did not differ on IQ ($p = 0.93$) or gender distribution ($p = 0.75$).

Comparison of ICA-derived DMN maps in children and young adults

We first characterized the DMN in children and young adults using ICA. ICA indicated that the DMN can be identified in both children and young adults, and consists of nodes in the mPFC, PCC, the left and right MTL, and the left and right AG nodes (Figure 1). A two sample t-test revealed that compared to young adults, children showed significantly weaker DMN connectivity and decreased spatial extent ($p < 0.01$, FDR corrected) in the mPFC but not in the PCC, MTL or the AG. Compared to young adults, children did not show greater network connectivity nor increased spatial extent in any brain region within the DMN.

Comparison of functional connectivity within the DMN in children and young adults

To further investigate group differences in ICA maps, we analyzed regional connectivity between the PCC, mPFC, MTL and the AG nodes of the DMN. Significant functional connectivity between each of these pairs of nodes was observed for both the child and young adult groups ($p < 0.001$, FDR corrected). In particular, strong functional connectivity between left and right MTL ($r_{children} = 0.53$, $r_{adults} = 0.58$), and between left and right AG ($r_{children} = 0.45$, $r_{adults} = 0.47$) was observed in both children and young adults. However, children showed significantly lower functional connectivity between the PCC and the mPFC than young adults ($p < 0.01$, FDR corrected). Partial correlation analysis revealed that this difference was significant ($p < 0.01$, FDR corrected) even after controlling for the influence of other nodes of the DMN (bilateral MTL and bilateral AG) and five other consistently detected large-scale brain networks -- salience, right executive control, left executive control, visual and sensorimotor network, as shown in Figure 2A. No other DMN nodes showed significant group differences in functional connectivity (Figure 3A, 4A). Additionally, we compared within hemisphere connectivity in each group. In children and young adults, no differences between PCC-right MTL and PCC-left MTL functional connectivity were observed ($p_{children} = 0.38$, $p_{adults} = 0.83$). Similar results were observed when PCC-right AG and PCC-left AG were compared in each group ($p_{children} = 0.12$, $p_{adults} = 0.34$).

Comparison of gray and white matter within the DMN in children and young adults

VBM revealed greater gray matter and lower white matter volume in children compared to young adults in several brain areas. DMN-related gray matter differences were observed in the PCC and mPFC (Figure 2B). White matter differences were observed in the dorsal cingulum "cingulate gyrus" tract, which connects the PCC and mPFC (Figure 2C) as well as left cingulum "hippocampus" tract, which connects the PCC and left MTL (Figure 3C). No group differences were found in the right cingulum tract connecting the PCC and right MTL (Figure 4C). Children did not show lower gray matter or greater white matter volumes in any brain region examined.

Comparison of DTI connectivity within the DMN in children and young adults

White matter tracts connecting the PCC to the mPFC and the MTL were detected in individual participants, as shown in Figure 5. Tracts connecting the PCC and mPFC were detected in all 33 participants for whom DTI data was available. PCC to right MTL tracts were detected in all 15 young adults and in 17 out of 18 children. PCC to left MTL tracts were detected in all 15 young adults, but in only 7 of 18 children. No tracts directly connecting the mPFC to the MTL were detected in either group.

The fiber density (number of fibers per unit area) of the PCC-mPFC tracts was significantly lower in children compared to young adults ($p < 0.001$), as shown in Figure 2D. Compared to young adults, children also showed significantly lower fiber density in the PCC-left MTL tracts ($p < 0.001$) (Figure 3D). This difference was significant even after excluding the subjects in which the PCC-left MTL tracts were not detected. There were no group differences in the fiber density of PCC-right MTL tracts (Figure 4D).

The mean FA value also showed similar differences between the two subject groups. The mean FA of the PCC-mPFC tracts was significantly lower in children compared to young adults ($p << 0.0001$) (Figure 2D). Compared to young adults, children also showed significantly lower mean FA along the PCC-left MTL tracts ($p < 0.01$) (Figure 3D). There were no group differences in the mean FA of the PCC-right MTL tracts (Figure 4D).

Replication and robustness of structural connectivity findings within the DMN in children

To determine if our novel structural connectivity findings, particularly the laterality effects observed in PCC to MTL fiber tracts in children, were robust (reproducible across datasets) we repeated the DTI analyses described in the main text on an independent dataset. This dataset was comprised of 10 subjects (5 males, 5 females) ranging in age from 7 to 9 (mean age 8.1) with an IQ range of 91 to 131 (mean IQ: 114). These subjects did not differ from the 23 children used in the original analyses, in age or IQ. Each subject underwent a structural, DTI, and resting-state fMRI scan. The parameters used for these scans were identical to those used for scanning participants that were examined in the original analyses. Results obtained from analyzing DTI data obtained from these 10 children were consistent with the original analyses: the PCC to mPFC fiber tracts were readily detected in all the children, the PCC to right MTL fiber tracts were detected in all but one children, while less than half the children (3 out of 10) showed PCC to left MTL fiber tracts.

Comparison of function-structure relationships within the DMN in children and young adults

Next, we examined the relationship between functional and structural connectivity within the DMN. We found that resting-state functional connectivity and fiber density between the PCC- and the mPFC were significantly positively correlated in young adults ($r = 0.57$; $p < 0.05$) but not in children ($r = 0.21$; $p = 0.4$), as shown in Figure 2E. This correlation was significant for the two groups combined ($r = 0.5$; $p < 0.05$). No significant correlation between functional connectivity and fiber density between the PCC and left or right MTL was observed in either

group (Figure 3E, 4E). This correlation was insignificant even after excluding the subjects in which the PCC-MTL fibers were not detected.

A similar relationship between DMN resting-state functional connectivity and structural connectivity was observed when mean FA was used as a measure of structural connectivity instead of fiber density. Specifically, we found that resting-state functional connectivity and mean FA between the PCC- and the mPFC were significantly positively correlated in young adults ($r = 0.62$; $p < 0.05$) but not in children ($r = 0.26$; $p = 0.28$). This correlation was significant for the two groups combined ($r = 0.53$; $p < 0.05$). No significant correlation between functional connectivity and mean FA between the PCC and left or right MTL was observed in either group. This correlation was insignificant even after excluding the subjects in which the PCC-MTL fibers were not detected.

Discussion

The human brain undergoes protracted structural and functional development (Barnea-Goraly et al., 2005; Sowell et al., 2003; Supekar et al., 2009). Most previous studies have focused on local changes in gray and white matter (Sowell et al., 2003), thus less is known about the maturation of functional circuits in the developing human brain. The DMN is a core network implicated in self-referential mental activity and social cognition, and understanding its developmental trajectory is important for clarifying how cognitive functions associated with this network mature with age. We found that the DMN undergoes significant developmental changes in functional and structural connectivity between childhood and adulthood. Our study pinpoints which specific DMN links are structurally and functionally mature by ages 7–9 and which links show a more protracted developmental trajectory. Importantly, our results also show that functional connectivity in children can reach adult-like levels even in the presence of weak structural connectivity. Convergent structural and functional connectivity analyses suggest that PCC-mPFC connectivity along the cingulum bundle is the most immature link in the DMN of children.

Maturation of functional connectivity within the DMN

Recent developmental functional neuroimaging studies have suggested that the posterior nodes of the DMN, most notably the PCC, can be identified in infants as young as 2 weeks of age; this is followed by the emergence of other DMN nodes such as the mPFC and MTL (Fransson et al., 2007; Gao et al., 2009). Our results suggest that in 7–9 year old children -- , like in adults, -- the DMN is comprised of nodes within PCC, mPFC, bilateral MTL and bilateral AG. Direct comparison of DMN maps derived using ICA showed that children had reduced network connectivity and the spatial extent of the connected mPFC node was smaller. Partial-correlation analysis confirmed that functional connectivity between mPFC and PCC was significantly weaker in children even after discounting the effects of other DMN regions. These results are broadly consistent with previous findings of Fair and colleagues (Fair et al., 2008) but methodologically, it is worth noting here that in our study we computed functional connectivity as partial correlation controlling for the influence of other DMN nodes and five other major large-scale brain networks. As noted by van den Heuvel and colleagues (van den Heuvel et al., 2008), this partial correlation approach has significant advantages over the pure correlation approach employed in previous studies. In particular, our analysis allows the investigation of functional connectivity uncontaminated by other confounding nodes and networks. Our use of continuous resting-state fMRI data, rather than resting-state data extracted from inter-task rest periods, also reduces potential contamination by cognitive tasks. There were no developmental changes in functional connectivity between any of the other DMN regions. Of note, there were no group differences in functional connectivity between mPFC and AG, although the anatomical distance between these nodes is greater than that between mPFC and PCC. Thus,

while long-range functional connectivity is typically weaker in children (Fair et al., 2007; Supekar et al., 2009), our results demonstrate that this is not uniformly the case within all nodes of the DMN. These results indicate that PCC and mPFC is the only DMN link that undergoes significant developmental changes in functional connectivity between childhood and young adulthood. More generally, with the observed resting-state functional connectivity differences between IQ-matched groups and recent evidence suggesting a strong association between patterns of resting-state functional connectivity and IQ (van den Heuvel et al., 2009b), future research investigating this association in development will provide additional insights into the complex relationships between brain connectivity and cognitive performance. We note, however, that analyses along the lines of van den Heuvel et al. (van den Heuvel et al., 2009b) failed to find any relation between IQ and DMN activity in both adults and children.

Maturation of structural connectivity within the DMN

Mirroring the developmental changes in functional connectivity, the density of fiber tracts connecting PCC and mPFC was also lower in children than in young adults. Our finding of consistent white matter tracts along the cingulum bundle in adults is similar to previous DTI tractography studies (Greicius et al., 2008; van den Heuvel et al., 2008; van den Heuvel et al., 2009a). Here we show that children also showed reliable, yet fewer tracts linking the PCC and mPFC along the cingulum bundle. Immature structural connectivity in PCC-mPFC tracts in children may reflect continued myelination and structural organization of axonal tracts, which begins early in development and lasts well into adulthood (Gogtay et al., 2004; Thompson et al., 2005).

Although children did not show decreased functional connectivity between PCC and MTL in either hemisphere when compared to adults, we found significant lateralized differences in structural connectivity between these regions. Children showed significantly reduced fiber density between PCC and MTL in the left, but not right, hemisphere. This is the first report of lateralized differences in structural connectivity between PCC and MTL. To our knowledge, structural connectivity of the MTL and PCC has not been previously examined in children. Because of the novel and unexpected results, we sought to replicate the findings in an independent dataset. Replicating our original result, the majority of children did not show fiber tracts between PCC and left MTL whereas PCC to mPFC and PCC to right MTL were detected in all children. The functional implications of weak PPC-MTL connectivity in the left hemisphere remain to be investigated. Importantly, however, our results suggest that functional connectivity within this DMN link reaches adult-like levels even in the presence of weak structural connectivity. Additional analysis indicated that the left and right MTL are strongly coupled functionally in both children and adults, and further suggest that interhemispheric interactions (Stark et al., 2008) may contribute to the observed functional connectivity of the PCC and left MTL in children.

Maturation of function-structure relationships within the DMN

As discussed above, both functional and structural connectivity between PCC and mPFC were significantly weaker in children compared to young adults. Analysis of the relationship between structural and functional connectivity provides further insights into the maturation of the DMN. In young adults, functional connectivity, assessed using partial correlations, was significantly correlated with structural connectivity, assessed using both fiber density and FA. Children showed a weak, but non-significant positive correlation between functional and structural connectivity. This suggests that function-structure relationships between the PCC and mPFC nodes of the DMN become more stable with development. The emergence of structure-function relationships along the PCC-mPFC link in adults further suggests that the maturation of its functional connectivity depends on the maturation of white matter tracts within the cingulum bundle.

Despite the lack of structural connectivity as identified by DTI between PCC and left MTL in most children, functional connectivity as identified by resting-state fMRI between these regions was not weaker in children. Such intact functional connectivity may arise from the strong interhemispheric functional connectivity between right and left MTL. Previous resting-state fMRI (Stark et al., 2008) and intracranial EEG studies (Nir et al., 2008) have shown that homotopic regions in the two cerebral hemispheres tend to have a high degree of correlated activity. Consistent with this interpretation, we found that functional connectivity between left and right MTL was equally high in both children and adults. Furthermore, computer simulations and lesion studies both suggest that indirect connections can account for intact functional connectivity in the absence of direct structural connectivity (Honey et al., 2009; Uddin et al., 2008). Taken together, these findings suggest that functional maturation of connectivity within the PCC-MTL link can precede maturation of its structural connectivity. This, however, is not the case with PCC-mPFC connectivity, which showed both weak structural and functional connectivity in children.

More generally, our findings critically inform our understanding of how function-structure relations evolve with development. In spite of the increasing number of studies using resting-state functional connectivity methods, there exists controversy regarding the exact origin of this connectivity in adults (Cordes et al., 2001; Morcom and Fletcher, 2007; Shmueli et al., 2007). Recent studies have suggested that resting-state connectivity reflects underlying neural coupling and is not an artifact (Nir et al., 2007). Other studies have reported that resting-state functional connectivity observed in the human brain reflect underlying anatomical structure (Damoiseaux and Greicius, 2009; Greicius et al., 2008; Hagmann et al., 2008; Honey et al., 2009; Margulies et al., 2009; Skudlarski et al., 2008; van den Heuvel et al., 2008; van den Heuvel et al., 2009a). This association between function and structure has been observed to be most significant within the DMN (Hagmann et al., 2008; Skudlarski et al., 2008). Our findings provide further evidence regarding the existence of a strong relationship between function and structure between the PCC and mPFC nodes of the DMN in young adults and provide novel evidence that this relationship is immature in children.

Maturation of gray and white matter within the DMN

In order to further investigate anatomical changes underlying the development of the DMN, we examined gray and white matter differences within and between each node of the DMN. VBM analyses revealed prominent gray matter differences in both the PCC and the mPFC, with children having greater gray matter volume compared to young adults. In conjunction with this finding, the dorsal cingulum bundle connecting these regions showed decreased white matter. Our finding of increased gray matter within PCC and mPFC shows a pattern similar to that observed in other polysensory and association cortices (Shaw et al., 2008). Greater gray matter in children likely reflects exuberant synaptic connectivity, which is reduced by synaptic pruning during development (Thompson et al., 2005). Our finding of decreased white matter volume in the dorsal cingulum bundle connecting PCC and mPFC in children is remarkably consistent with our finding of decreased fiber density and mean FA along this pathway measured by DTI and more generally, with previous reports of delayed white matter maturation in children (Barnea-Goraly et al., 2005; Gogtay et al., 2004). These observations suggest that pruning of local circuits in PCC and mPFC, as well as macrostructural and microstructural changes in white matter tracts linking them, contribute to development of the DMN.

In addition to anatomical differences in the PCC and mPFC, we also observed white matter volume differences in the tracts linking the PCC with the MTL. Consistent with our findings of decreased fiber tracts linking PCC with left, but not right MTL, we found that only left MTL tracts in children showed decreased white matter volume. The convergence of DTI and VBM results provides further evidence of delayed maturation of PCC-MTL structural connectivity

deficits in children. Our combined analysis of tractography and morphometric measures provides additional confirmation of decreased white matter integrity in children along fibers connecting PCC, mPFC and left MTL nodes of the DMN.

Limitations

The main limitation of this study is that current methodological shortcomings of DTI do not allow reliable fiber tracking through regions with a high number of crossing fibers. While the functional connectivity between all DMN regions can be easily measured using resting-state fMRI, examining white matter tracts connecting these regions, particularly those linking the AG to other DMN nodes, is challenging. AG tracts connecting to the medial nodes of the DMN are likely to cross other larger tracts such as the superior longitudinal fasciculus and the arcuate fasciculus, and resolving crossing fibers using current tractography methods is difficult. Future studies that use innovative tractography methods (Behrens et al., 2007) that allow better resolution of crossing fibers, are required for a more comprehensive analysis of structural connectivity between all nodes of the DMN.

Conclusion

Each of the major nodes (PCC, mPFC, AG, MTL) of the DMN could be consistently detected in 7–9 year old children. We found that children had significantly weaker functional and structural connectivity between the anterior (mPFC) and posterior (PCC) nodes of the DMN. Both the PCC and the mPFC also showed gray volume differences, as well as prominent macrostructural and microstructural differences in the dorsal cingulum bundle that links these regions. Notably, functional connectivity was not uniformly weaker in children, as other DMN nodes did not show any functional deficits. One novel finding of this study is that structural connectivity between the PCC and left MTL was significantly weaker in children, even though functional connectivity did not differ from that of adults. We suggest that in this case, strong inter-hemispheric interaction between the left and right MTL may mitigate the effects of weak structural connectivity. Based on our findings, we hypothesize that maturation of the DMN, and in particular maturation of structural and functional connectivity between PCC and mPFC, plays an important role in the development of self- and social-cognitive functions that emerge during adolescence. Future longitudinal studies relating changes in structural and functional connectivity measures with changes in behavioral and cognitive assessments are needed to test this hypothesis.

More generally, our study demonstrates how quantitative analysis of functional and structural anatomy and connectivity allows us to characterize the heterogeneous development and maturation of functional brain networks. Such multimodal imaging analysis will be important for better understanding how local and large-scale anatomical changes shape and constrain typical and atypical cognitive development.

Abbreviations

DMN	Default-mode network
PCC	Posterior cingulate cortex
mPFC	Medial prefrontal cortex
MTL	Medial temporal lobes
fMRI	Functional magnetic resonance imaging
DTI	Diffusion tensor imaging
VBM	Voxel-based morphometry

Acknowledgments

We thank Leeza Kondos and Jose Anguiano for their assistance with data acquisition. This work was supported by the National Institutes of Health (HD047520, HD059205, NS058899 to VM); the National Science Foundation (BCS-0449927 to VM) and the Children's Health Research Program of the Lucille Packard Children's Hospital.

References

Alexander DC, Pierpaoli C, Basser PJ, Gee JC. Spatial transformations of diffusion tensor magnetic resonance images. IEEE Trans Med Imaging 2001;20:1131–1139. [PubMed: 11700739]

Amodio DM, Frith CD. Meeting of minds: the medial frontal cortex and social cognition. Nat Rev Neurosci 2006;7:268–277. [PubMed: 16552413]

Bammer R, Auer M, Keeling SL, Augustin M, Stables LA, Prokesch RW, Stollberger R, Moseley ME, Fazekas F. Diffusion tensor imaging using single-shot SENSE-EPI. Magn Reson Med 2002;48:128–136. [PubMed: 12111940]

Barnea-Goraly N, Menon V, Eckert M, Tamm L, Bammer R, Karchemskiy A, Dant CC, Reiss AL. White matter development during childhood and adolescence: A cross-sectional diffusion tensor imaging study. Cerebral Cortex 2005;15:1848–1854. [PubMed: 15758200]

Basser PJ. Inferring microstructural features and the physiological state of tissues from diffusion-weighted images. NMR Biomed 1995;8:333–344. [PubMed: 8739270]

Basser PJ, Pajevic S, Pierpaoli C, Duda J, Aldroubi A. In vivo fiber tractography using DT-MRI data. Magn Reson Med 2000;44:625–632. [PubMed: 11025519]

Basser PJ, Pierpaoli C. Microstructural and physiological features of tissues elucidated by quantitative-diffusion-tensor MRI. J Magn Reson B 1996;111:209–219. [PubMed: 8661285]

Beaulieu C. The basis of anisotropic water diffusion in the nervous system - a technical review. NMR Biomed 2002;15:435–455. [PubMed: 12489094]

Behrens TE, Berg HJ, Jbabdi S, Rushworth MF, Woolrich MW. Probabilistic diffusion tractography with multiple fibre orientations: What can we gain? NeuroImage 2007;34:144–155. [PubMed: 17070705]

Binder JR, Desai RH, Graves WW, Conant LL. Where Is the Semantic System? A Critical Review and Meta-Analysis of 120 Functional Neuroimaging Studies. Cereb Cortex. 2009

Biswal B, Yetkin FZ, Haughton VM, Hyde JS. Functional connectivity in the motor cortex of resting human brain using echo-planar MRI. Magn Reson Med 1995;34:537–541. [PubMed: 8524021]

Broyd SJ, Demanuele C, Debener S, Helps SK, James CJ, Sonuga-Barke EJ. Default-mode brain dysfunction in mental disorders: a systematic review. Neurosci Biobehav Rev 2009;33:279–296. [PubMed: 18824195]

Buckner RL, Carroll DC. Self-projection and the brain. Trends Cogn Sci 2007;11:49–57. [PubMed: 17188554]

Chambers CD, Payne JM, Stokes MG, Mattingley JB. Fast and slow parietal pathways mediate spatial attention. Nat Neurosci 2004;7:217–218. [PubMed: 14983182]

Conturo TE, Lori NF, Cull TS, Akbudak E, Snyder AZ, Shimony JS, McKinstry RC, Burton H, Raichle ME. Tracking neuronal fiber pathways in the living human brain. Proc Natl Acad Sci U S A 1999;96:10422–10427. [PubMed: 10468624]

Cordes D, Haughton VM, Arfanakis K, Carew JD, Turski PA, Moritz CH, Quigley MA, Meyerand ME. Frequencies contributing to functional connectivity in the cerebral cortex in "resting-state" data. AJNR Am J Neuroradiol 2001;22:1326–1333. [PubMed: 11498421]

Damoiseaux JS, Greicius MD. Greater than the sum of its parts: a review of studies combining structural connectivity and resting-state functional connectivity. Brain Struct Funct 2009;213:525–533. [PubMed: 19565262]

Damoiseaux JS, Rombouts SA, Barkhof F, Scheltens P, Stam CJ, Smith SM, Beckmann CF. Consistent resting-state networks across healthy subjects. Proc Natl Acad Sci U S A 2006;103:13848–13853. [PubMed: 16945915]

De Luca M, Smith S, De Stefano N, Federico A, Matthews PM. Blood oxygenation level dependent contrast resting state networks are relevant to functional activity in the neocortical sensorimotor system. Exp Brain Res 2005;167:587–594. [PubMed: 16284751]

Fair DA, Cohen AL, Dosenbach NU, Church JA, Miezin FM, Barch DM, Raichle ME, Petersen SE, Schlaggar BL. The maturing architecture of the brain's default network. Proc Natl Acad Sci U S A 2008;105:4028–4032. [PubMed: 18322013]

Fair DA, Dosenbach NU, Church JA, Cohen AL, Brahmbhatt S, Miezin FM, Barch DM, Raichle ME, Petersen SE, Schlaggar BL. Development of distinct control networks through segregation and integration. Proc Natl Acad Sci U S A 2007;104:13507–13512. [PubMed: 17679691]

Fox MD, Snyder AZ, Vincent JL, Corbetta M, Van Essen DC, Raichle ME. The human brain is intrinsically organized into dynamic, anticorrelated functional networks. Proc Natl Acad Sci U S A 2005;102:9673–9678. [PubMed: 15976020]

Fransson P, Skiold B, Horsch S, Nordell A, Blennow M, Lagercrantz H, Aden U. Resting-state networks in the infant brain. Proc Natl Acad Sci U S A 2007;104:15531–15536. [PubMed: 17878310]

Gao W, Zhu H, Giovanello KS, Smith JK, Shen D, Gilmore JH, Lin W. Evidence on the emergence of the brain's default network from 2-week-old to 2-year-old healthy pediatric subjects. Proc Natl Acad Sci U S A. 2009

Glover GH, Lai S. Self-navigated spiral fMRI: interleaved versus single-shot. Magnetic resonance in medicine : official journal of the Society of Magnetic Resonance in Medicine / Society of Magnetic Resonance in Medicine 1998;39:361–368. [PubMed: 9498591]

Glover GH, Law CS. Spiral-in/out BOLD fMRI for increased SNR and reduced susceptibility artifacts. Magn Reson Med 2001;46:515–522. [PubMed: 11550244]

Gogtay N, Giedd JN, Lusk L, Hayashi KM, Greenstein D, Vaituzis AC, Nugent TF 3rd, Herman DH, Clasen LS, Toga AW, Rapoport JL, Thompson PM. Dynamic mapping of human cortical development during childhood through early adulthood. Proc Natl Acad Sci U S A 2004;101:8174–8179. [PubMed: 15148381]

Good CD, Johnsrude IS, Ashburner J, Henson RN, Friston KJ, Frackowiak RS. A voxel-based morphometric study of ageing in 465 normal adult human brains. NeuroImage 2001;14:21–36. [PubMed: 11525331]

Greicius MD, Krasnow B, Reiss AL, Menon V. Functional connectivity in the resting brain: a network analysis of the default mode hypothesis. Proceedings of the National Academy of Sciences of the United States of America 2003;100:253–258. [PubMed: 12506194]

Greicius MD, Srivastava G, Reiss AL, Menon V. Default-mode network activity distinguishes Alzheimer's disease from healthy aging: evidence from functional MRI. Proc Natl Acad Sci U S A 2004;101:4637–4642. [PubMed: 15070770]

Greicius MD, Supekar K, Menon V, Dougherty RF. Resting-State Functional Connectivity Reflects Structural Connectivity in the Default Mode Network. Cereb Cortex. 2008

Hagmann P, Cammoun L, Gigandet X, Meuli R, Honey CJ, Wedeen VJ, Sporns O. Mapping the structural core of human cerebral cortex. PLoS Biol 2008;6:e159. [PubMed: 18597554]

Harrison BJ, Pujol J, Lopez-Sola M, Hernandez-Ribas R, Deus J, Ortiz H, Soriano-Mas C, Yucel M, Pantelis C, Cardoner N. Consistency and functional specialization in the default mode brain network. Proc Natl Acad Sci U S A 2008;105:9781–9786. [PubMed: 18621692]

Hayasaka S, Phan KL, Liberzon I, Worsley KJ, Nichols TE. Nonstationary cluster-size inference with random field and permutation methods. NeuroImage 2004;22:676–687. [PubMed: 15193596]

Honey CJ, Sporns O, Cammoun L, Gigandet X, Thiran JP, Meuli R, Hagmann P. Predicting human resting-state functional connectivity from structural connectivity. Proc Natl Acad Sci U S A 2009;106:2035–2040. [PubMed: 19188601]

Jones DK. The effect of gradient sampling schemes on measures derived from diffusion tensor MRI: a Monte Carlo study. Magn Reson Med 2004;51:807–815. [PubMed: 15065255]

Kelly AM, Di Martino A, Uddin LQ, Shehzad Z, Gee DG, Reiss PT, Margulies DS, Castellanos FX, Milham MP. Development of anterior cingulate functional connectivity from late childhood to early adulthood. Cereb Cortex 2009;19:640–657. [PubMed: 18653667]

Kelly AM, Uddin LQ, Biswal BB, Castellanos FX, Milham MP. Competition between functional brain networks mediates behavioral variability. NeuroImage 2008;39:527–537. [PubMed: 17919929]

Lenroot RK, Giedd JN. Brain development in children and adolescents: insights from anatomical magnetic resonance imaging. Neurosci Biobehav Rev 2006;30:718–729. [PubMed: 16887188]

Liu Y, Liang M, Zhou Y, He Y, Hao Y, Song M, Yu C, Liu H, Liu Z, Jiang T. Disrupted small-world networks in schizophrenia. Brain 2008;131:945–961. [PubMed: 18299296]

Margulies DS, Vincent JL, Kelly C, Lohmann G, Uddin LQ, Biswal BB, Villringer A, Castellanos FX, Milham MP, Petrides M. Precuneus shares intrinsic functional architecture in humans and monkeys. Proc Natl Acad Sci U S A 2009;106:20069–20074. [PubMed: 19903877]

Milner B. The medial temporal-lobe amnesic syndrome. Psychiatr Clin North Am 2005;28:599–611. 609. [PubMed: 16122569]

Morcom AM, Fletcher PC. Does the brain have a baseline? Why we should be resisting a rest. NeuroImage 2007;37:1073–1082.

Mori S, Crain BJ, Chacko VP, van Zijl PC. Three-dimensional tracking of axonal projections in the brain by magnetic resonance imaging. Ann Neurol 1999;45:265–269. [PubMed: 9989633]

Nir Y, Fisch L, Mukamel R, Gelbard-Sagiv H, Arieli A, Fried I, Malach R. Coupling between neuronal firing rate, gamma LFP, and BOLD fMRI is related to interneuronal correlations. Curr Biol 2007;17:1275–1285. [PubMed: 17686438]

Nir Y, Mukamel R, Dinstein I, Privman E, Harel M, Fisch L, Gelbard-Sagiv H, Kipervasser S, Andelman F, Neufeld MY, Kramer U, Arieli A, Fried I, Malach R. Interhemispheric correlations of slow spontaneous neuronal fluctuations revealed in human sensory cortex. Nat Neurosci 2008;11:1100–1108. [PubMed: 19160509]

Pajevic S, Aldroubi A, Basser PJ. A continuous tensor field approximation of discrete DT-MRI data for extracting microstructural and architectural features of tissue. J Magn Reson 2002;154:85–100. [PubMed: 11820830]

Polli FE, Barton JJ, Cain MS, Thakkar KN, Rauch SL, Manoach DS. Rostral and dorsal anterior cingulate cortex make dissociable contributions during antisaccade error commission. Proc Natl Acad Sci U S A 2005;102:15700–15705. [PubMed: 16227444]

Press, WH. Numerical recipes in C++ : the art of scientific computing. 2nd ed. Cambridge, UK; New York: Cambridge University Press; 2002.

Raichle ME, MacLeod AM, Snyder AZ, Powers WJ, Gusnard DA, Shulman GL. A default mode of brain function. Proc Natl Acad Sci U S A 2001;98:676–682. [PubMed: 11209064]

Salvador R, Suckling J, Coleman MR, Pickard JD, Menon D, Bullmore E. Neurophysiological architecture of functional magnetic resonance images of human brain. Cereb Cortex 2005;15:1332–1342. [PubMed: 15635061]

Seeley WW, Menon V, Schatzberg AF, Keller J, Glover GH, Kenna H, Reiss AL, Greicius MD. Dissociable intrinsic connectivity networks for salience processing and executive control. Journal of Neuroscience 2007;27:2349–2356. [PubMed: 17329432]

Shaw P, Kabani NJ, Lerch JP, Eckstrand K, Lenroot R, Gogtay N, Greenstein D, Clasen L, Evans A, Rapoport JL, Giedd JN, Wise SP. Neurodevelopmental trajectories of the human cerebral cortex. J Neurosci 2008;28:3586–3594. [PubMed: 18385317]

Shmueli K, van Gelderen P, de Zwart JA, Horovitz SG, Fukunaga M, Jansma JM, Duyn JH. Low-frequency fluctuations in the cardiac rate as a source of variance in the resting-state fMRI BOLD signal. NeuroImage 2007;38:306–320. [PubMed: 17869543]

Shulman GL, Fiez JA, Corbetta M, Buckner RL, Miezin FM, Raichle ME, Petersen SE. Common Blood Flow Changes across Visual Tasks: II. Decreases in Cerebral Cortex. Journal of Cognitive Neuroscience 1997;9:648.

Skudlarski P, Jagannathan K, Calhoun VD, Hampson M, Skudlarska BA, Pearlson G. Measuring brain connectivity: diffusion tensor imaging validates resting state temporal correlations. NeuroImage 2008;43:554–561. [PubMed: 18771736]

Sowell ER, Peterson BS, Thompson PM, Welcome SE, Henkenius AL, Toga AW. Mapping cortical change across the human life span. Nat Neurosci 2003;6:309–315. [PubMed: 12548289]

Spreng RN, Mar RA, Kim AS. The common neural basis of autobiographical memory, prospection, navigation, theory of mind, and the default mode: a quantitative meta-analysis. J Cogn Neurosci 2009;21:489–510. [PubMed: 18510452]

Stark DE, Margulies DS, Shehzad ZE, Reiss P, Kelly AM, Uddin LQ, Gee DG, Roy AK, Banich MT, Castellanos FX, Milham MP. Regional variation in interhemispheric coordination of intrinsic hemodynamic fluctuations. J Neurosci 2008;28:13754–13764. [PubMed: 19091966]

Sun FT, Miller LM, D'Esposito M. Measuring interregional functional connectivity using coherence and partial coherence analyses of fMRI data. NeuroImage 2004;21:647–658. [PubMed: 14980567]

Supekar K, Musen M, Menon V. Development of large-scale functional brain networks in children. PLoS Biol 2009;7:e1000157. [PubMed: 19621066]

Thompson PM, Sowell ER, Gogtay N, Giedd JN, Vidal CN, Hayashi KM, Leow A, Nicolson R, Rapoport JL, Toga AW. Structural MRI and brain development. Int Rev Neurobiol 2005;67:285–323. [PubMed: 16291026]

Uddin LQ, Mooshagian E, Zaidel E, Scheres A, Margulies DS, Kelly AM, Shehzad Z, Adelstein JS, Castellanos FX, Biswal BB, Milham MP. Residual functional connectivity in the split-brain revealed with resting-state functional MRI. Neuroreport 2008;19:703–709. [PubMed: 18418243]

van den Heuvel M, Mandl R, Luigjes J, Hulshoff Pol H. Microstructural organization of the cingulum tract and the level of default mode functional connectivity. J Neurosci 2008;28:10844–10851. [PubMed: 18945892]

van den Heuvel MP, Mandl RC, Kahn RS, Hulshoff Pol HE. Functionally linked resting-state networks reflect the underlying structural connectivity architecture of the human brain. Hum Brain Mapp 2009a;30:3127–3141. [PubMed: 19235882]

van den Heuvel MP, Stam CJ, Kahn RS, Hulshoff Pol HE. Efficiency of functional brain networks and intellectual performance. J Neurosci 2009b;29:7619–7624. [PubMed: 19515930]

Weissman DH, Roberts KC, Visscher KM, Woldorff MG. The neural bases of momentary lapses in attention. Nat Neurosci 2006;9:971–978. [PubMed: 16767087]

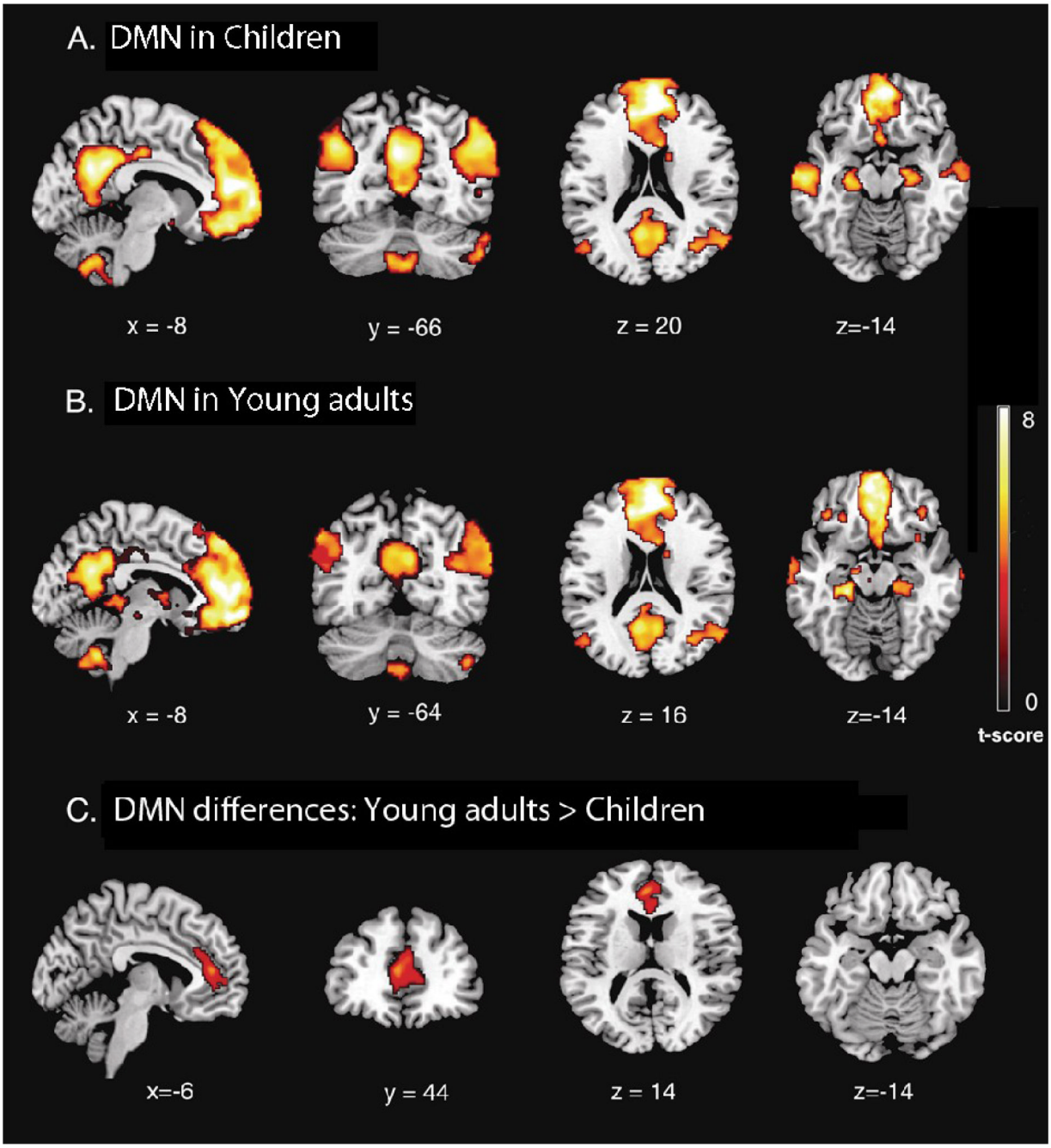

Figure 1. Weaker DMN activity in children

Default mode network (DMN) in (**A**) children, and (**B**) young adults. (**C**) shows results of a two-sample *t* test contrasting the DMN in young adults vs. children. Both groups show activity in posterior cingulate cortex (PCC), medial prefrontal cortex (mPFC), medial temporal lobe (MTL), and angular gyrus (AG). Compared to young adults, children showed reduced activity in the mPFC ($p < 0.01$). Compared to young adults, children did not show greater DMN activity in any brain region.

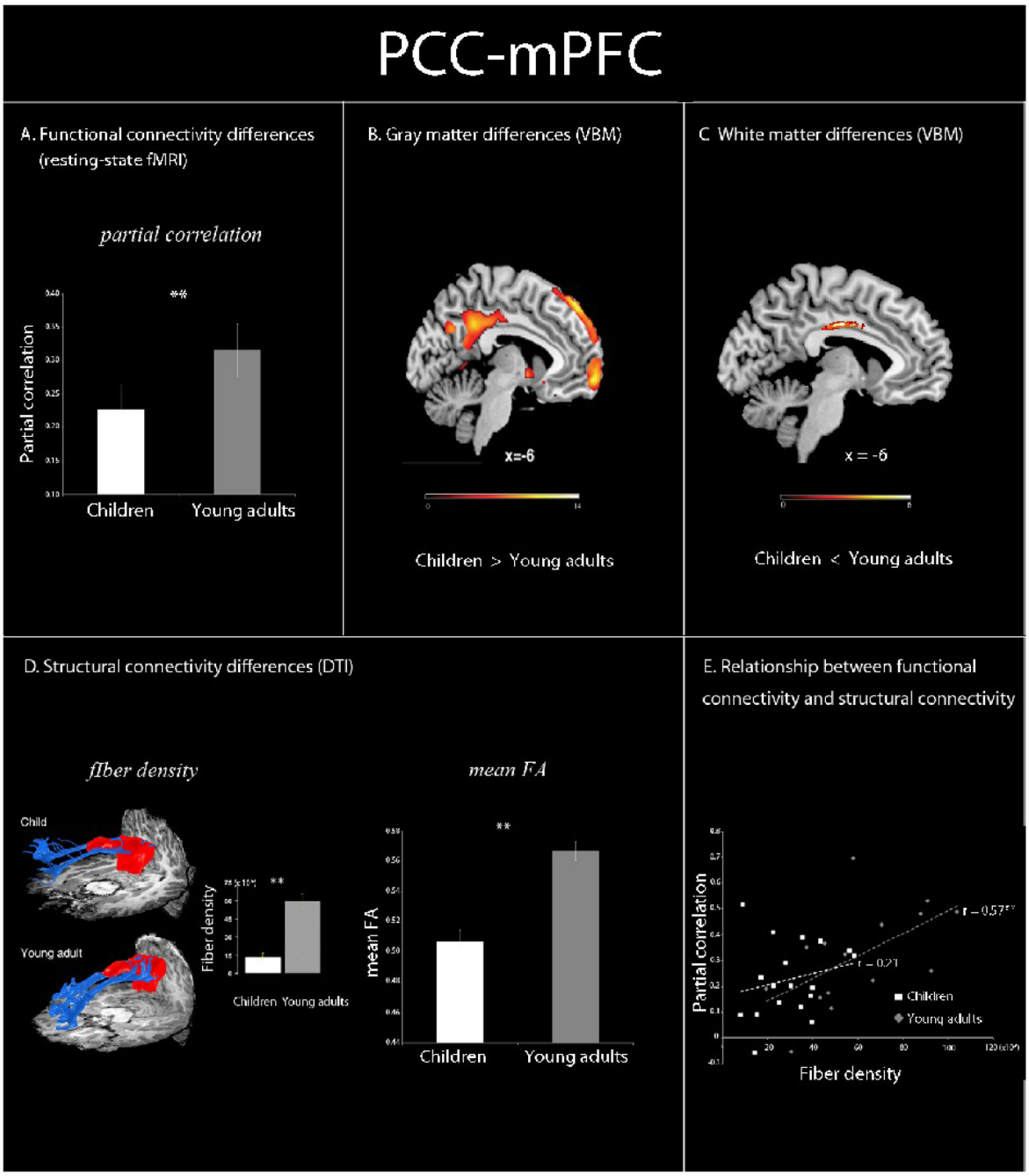

Figure 2. Maturation of DMN: PCC-mPFC connectivity

(**A**) Functional connectivity between PCC and mPFC was significantly weaker in children, compared to young adults ($p < 0.01$, indicated by **). Functional connectivity was assessed using partial correlation between specific nodes of the default mode network (DMN) after controlling for the influence of other nodes of the DMN and five non-DMN brain networks. (**B**) Greater gray matter volume in the PCC and mPFC was observed in children, compared to young adults. (**C**) Lower white matter volume was observed in children within the cingulum (cingulate gyrus), which connects the PCC and mPFC. (**D**) DTI tractography of fiber tracts connecting PCC to mPFC (blue tracts). Fiber density, the number of fibers per unit area between the PCC to mPFC, was significantly lower in children, compared to young adults ($p < 0.001$,

indicated by **). The mean FA of the PCC-mPFC fibers was significantly lower in children compared to young adults ($p << 0.0001$, indicated by **). (**E**) Functional connectivity, assessed using partial correlations between the PCC and mPFC, and structural connectivity, assessed using DTI-based measures of fiber density showed positive correlation in young adults ($r = 0.57$; $p < 0.05$, indicated by **) but not in children ($r = 0.21$; $p = 0.4$). A similar relationship between PCC-mPFC functional connectivity and structural connectivity was observed when mean FA was used as a measure of structural connectivity instead of fiber density (data not shown).

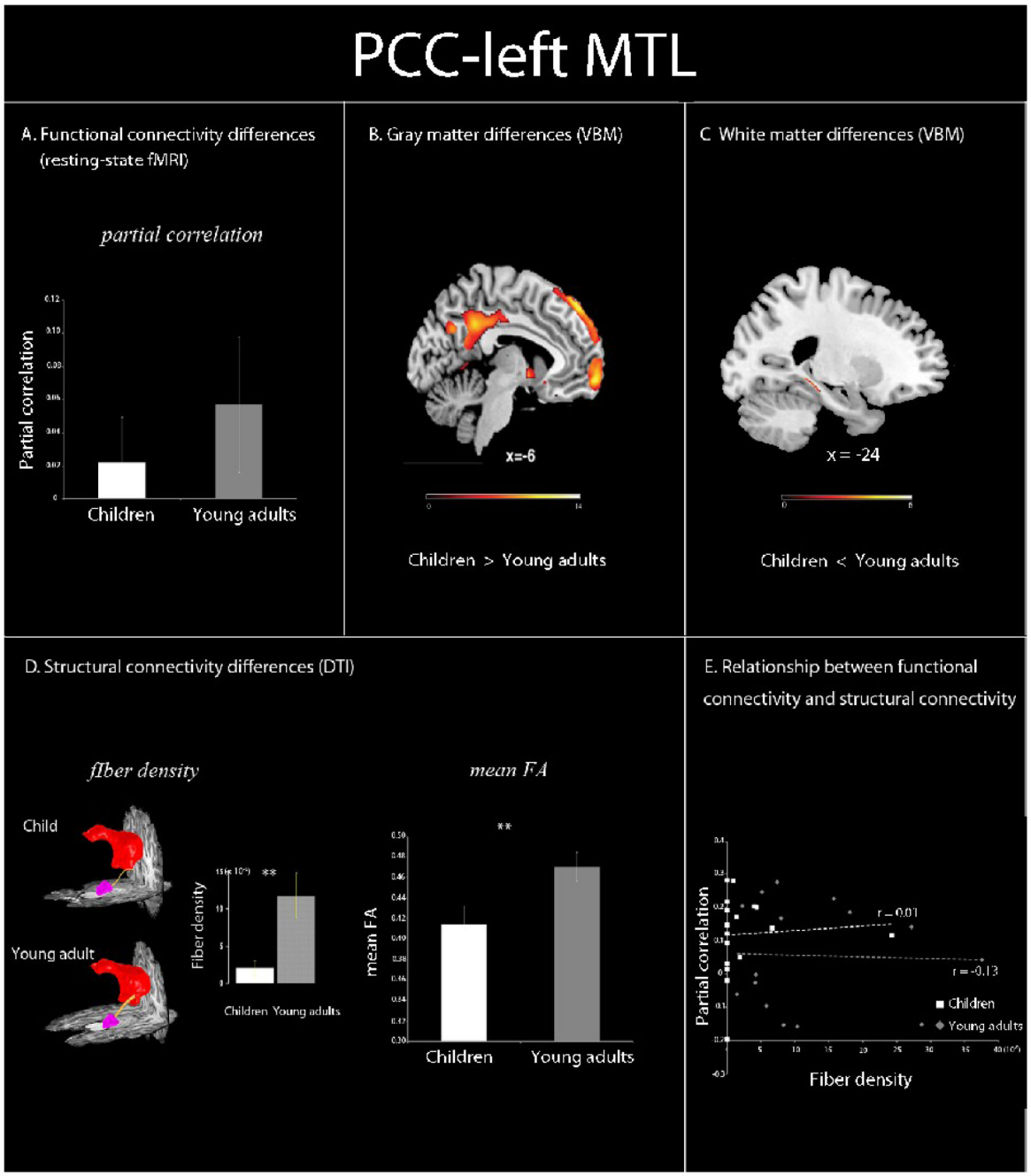

Figure 3. Maturation of DMN: PCC-left MTL connectivity

(**A**) No significant group difference in functional connectivity between PCC and left MTL was observed. Functional connectivity was assessed using partial correlation between specific nodes of the default mode network (DMN) after controlling for the influence of other nodes of the DMN and five non-DMN brain networks. (**B**) Greater gray matter volume in the PCC but not the left MTL was observed in children, compared to young adults. (**C**) Lower white matter volume was observed in children within the left cingulum (hippocampus), which connects the PCC and left MTL. (**D**) DTI tractography of fiber tracts connecting PCC to left MTL (yellow tracts). Fiber density, the number of fibers per unit area between the PCC to left MTL, was significantly lower in children, compared to young adults ($p < 0.001$, indicated by

). The mean FA of the PCC-leftMTL fibers was significantly lower in children compared to young adults ($p < 0.001$, indicated by **). (E**) No significant correlation between functional connectivity, assessed using partial correlations and structural connectivity, assessed using DTI-based measures of fiber density between the PCC and left MTL was observed in either group. A similar relationship between PCC-left MTL functional connectivity and structural connectivity was observed when mean FA was used as a measure of structural connectivity instead of fiber density (data not shown).

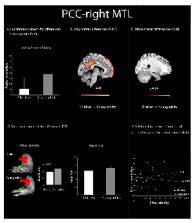

Figure 4. Maturation of DMN: PCC-right MTL connectivity

(**A**) No significant group difference in functional connectivity between PCC and right MTL was observed. Functional connectivity was assessed using partial correlation between specific nodes of the default mode network (DMN) after controlling for the influence of other nodes of the DMN and five non-DMN brain networks. (**B**) Greater gray matter volume in the PCC but not the right MTL was observed in children, compared to young adults. (**C**) No white matter volume group differences were found in the right cingulum (hippocampus), which connects the PCC and right MTL. (**D**) DTI tractography of fiber tracts connecting PCC to right MTL (yellow tracts). No significant group differences in the density of fibers connecting PCC to right MTL were observed. No significant group differences in the mean FA of PCC-rightMTL fibers were observed (**E**) No significant correlation between functional connectivity, assessed using partial correlations and structural connectivity, assessed using DTI-based measures of fiber density between the PCC and right MTL was observed in either group. A similar relationship between PCC-rightMTL functional connectivity and structural connectivity was observed when mean FA was used as a measure of structural connectivity instead of fiber density (data not shown)

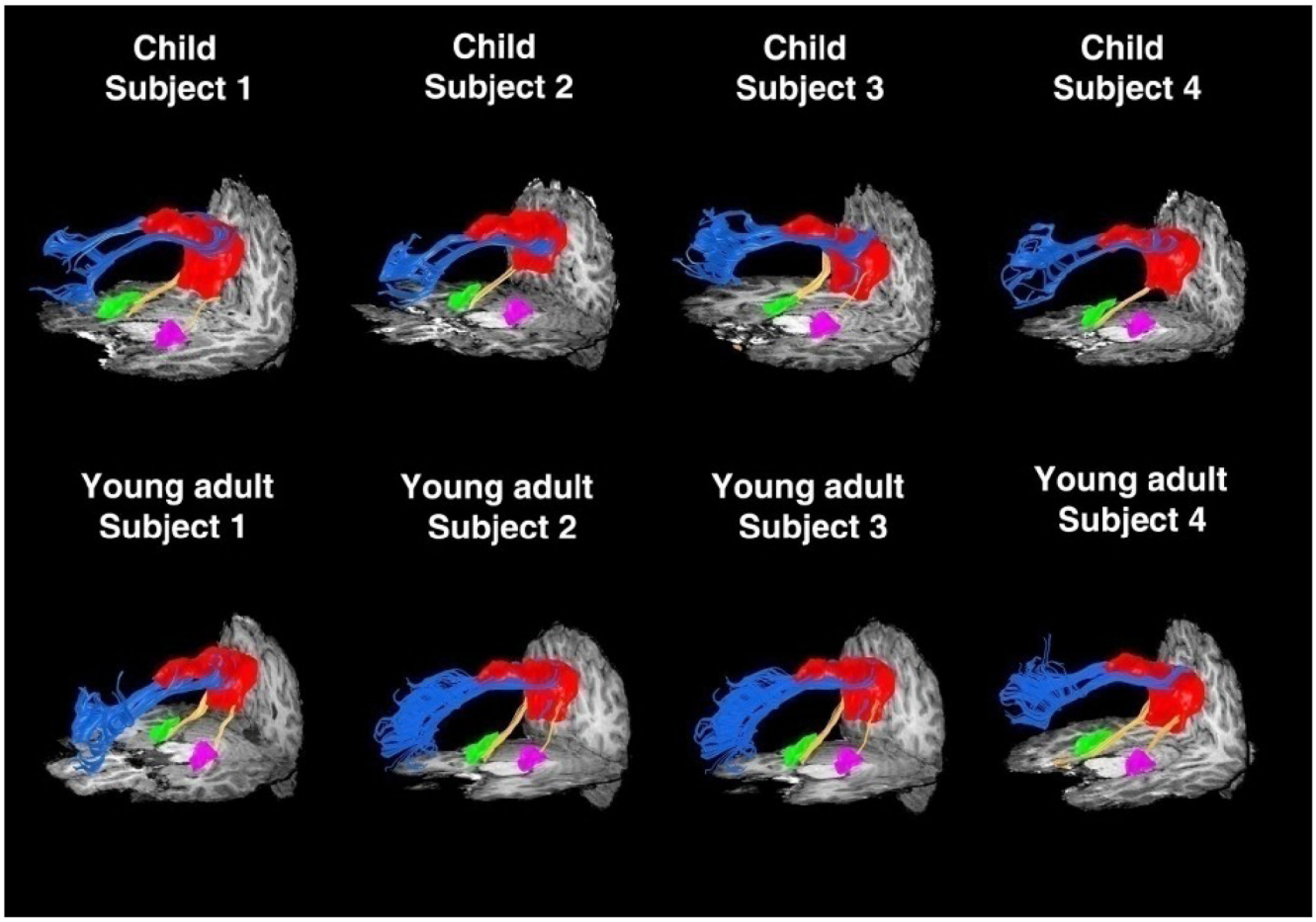

Figure 5. Individual subject fiber tracts between DMN regions in children and young adults

Representative single-subject DTI tractography in four children and four young adults showing fiber tracts linking the PCC (shown in red), mPFC, and left (purple) and right MTL (green). Both children and adults showed fiber tracts from the mPFC that enter the more rostral aspect of the PCC (shown in blue), and tracts from the MTL that enter the more caudal aspect of the PCC (shown in yellow). Only half of the children showed tracts between PCC and left MTL. There were no tracts connecting the mPFC to the MTL.

Table 1

Demographic Information

The two groups did not differ on IQ or gender distribution.

	Children (n = 23)	**Young adults (n = 22)**
Age	7.95** (range: 7 to 9)	20.40** (range: 19 to 22)
Gender	10 males, 13 females	11 males, 11 females
IQ	112 (range: 88 to 137)	112 (range:97 to 137)
Years of education	2.52** (range: 2 to 3)	14.5** (range: 13 to 16)

** Significant group differences $p << 0.01$

Table 2

Scanner Movement Parameters

The two groups did not differ on any of the six motion parameters (x, y, z, pitch, roll, yaw).

	Children (n = 23)	**Young adults (n = 22)**	**p value**
Translation (x, y, z): range(in mm)	0.335, 0.335, 0.99	0.267, 0.307, 0.39	0.41, 0.5, 0.39
Rotation (pitch, roll, yaw): range(in degrees)	0.021, 0.01, 0.01	0.01, 0.005, 0.006	0.19, 0.12, 0.20